D38

N79-17513

MANUAL CONTROL OF YAW MOTION WITH COMBINED VISUAL AND VESTIBULAR CUES *

Greg L. Zacharias and Laurence R. Young

Man Vehicle Laboratory
Department of Aeronautics and Astronautics
Massachusetts Institute of Technology

ABSTRACT

Measurements are made of manual control performance in the closed-loop task of nulling perceived self-rotation velocity about an earth-vertical axis. Self-velocity estimation was modelled as a function of the simultaneous presentation of vestibular and peripheral visual field motion cues. Based on measured low-frequency operator behavior in three visual field environments, a parallel channel linear model is proposed which has separate visual and vestibular pathways summing in a complementary manner. A correction to the frequency responses is provided by a separate measurement of manual control performance in an analogous visual pursuit nulling task. The resulting dual-input describing function for motion perception dependence on combined cue presentation supports the complementary model, in which vestibular cues dominate sensation at frequencies above 0.05 Hz. The describing function model is extended by the proposal of a non-linear cue conflict model, in which cue weighting depends on the level of agreement between visual and vestibular cues.

1.0 Introduction

Considerable attention has been directed toward the problem of understanding how our sense of self-motion is determined by the sensory cues available to us. The concentration on vestibular sensation has met with a fair degree of success in developing descriptive models which predict sensation as a function of actual motion. Efforts directed at determining how motion cues in the peripheral visual field affect sensation have emphasized the qualitative aspects of the cues which best elicit motion illusions, although some work has also been directed toward explaining the dynamics of such illusions. A natural extension of both visual and vestibular studies is understanding response to simultaneous cue presentation; the research reported here is directed toward that goal.

Neurophysiological studies (1,2,3,4,5) of combined visual-vestibular cue presentation point to a mixing of the two sensory modalities at the level of the vestibular nucleus, in a manner which is consistent with normal head motion in an inertially fixed visual field environment. That is, a unit which responds in an excitatory manner to right head motions responds similarly to left visual field motions, although the response dynamics are clearly different in the two cases. In the dark, a step in angular velocity of the head results in a rapid rise in firing rate followed by a nearly exponential decay, characteristic of semicircular canal transduction. In contrast, a step in visual field velocity results, after a delay, in a slow rise to a new steady state firing rate, a rate which is held for as long as the visual stimulus continues. The implication, of course, is that the visual motion cue provides DC velocity information to augment the AC transduction characteristics of the canals, thereby producing a wide-band motion sensation system.

Psychophysical studies (6,7,8,9) show sensation to roughly parallel unit behavior in response to separate and combined cue presentations. Specifically, a circularvection (CV) illusion can be generated in a subject when he is seated upright and presented with a peripheral visual field which rotates at a constant velocity about an earth vertical axis. Even though he is motionless, the subject eventually feels himself rotating at constant velocity and perceives the field to be fixed in space. The differential velocity transfer takes about 10 seconds (6). Since the response time is so long, when compared with visual motion detection times which must be orders of magnitude smaller, one is tempted to implicate the canal dynamics in the sensory processing. How this is to be done is not clear at present, although the framework of the "conflict model" proposed by Young (10) appears to be a logical starting point for a functional modelling effort.

2.0 Background

There have been several qualitative studies and a few quantitative attempts to measure the interaction dynamics of sensation in response to combined cue presentation. In one study (9), velocity and acceleration detection indications were made by subjects in response to earth-vertical yaw-axis rotational cues. These consisted of angular acceleration pulses in conjunction with the presentation of a visual field moving at a constant angular velocity with respect to the subject. A pulse was considered confirming when it was in the direction of the induced circularvection and conflicting when in the opposite direction. The study showed the following. First, subjective velocity was found to be biased in the direction of the induced CV and expected vestibular response. Second, detection of a confirming pulse generally led to a moderate increase in subjective velocity, whereas a conflicting pulse, if detected, resulted in a marked decrease.

A similar study conducted by Berthoz et al (11) combined linear fore-aft acceleration pulses with linear visual field motion. They found qualitatively the same subjective dependence on dual cue presentation: a slow rise in sensation when only visual cues were presented, and a subjective velocity bias due to constant field velocity. Vestibular pulse detection performance was also similar, the study showing detection to be degraded during linearvection.

It is appropriate to note that both of the above studies used a constant velocity visual field and thus were unable to provide a closer look at visual channel response dynamics. In effect, what was studied was the "vestibular" transfer function, and its dependence on visual motion cues.

The objective of the research reported here is to develop a simplified functional model of motion sensation dependence on combined visual and motion cues, thus directly extending the results of the work just described. The study is restricted to yaw-axis motion about an earth-vertical in order to take advantage of past work on this type of motion, and to avoid possible complications of otolith involvement in subjective response.

3.0 General Experimental Approach

To avoid the possible pitfalls of using subjective magnitude estimation (12) to measure motion sensation, a compensatory tracking task was devised to give a subject control over his own (sensed) velocity, with a task objective of keeping himself (apparently) fixed in space. Visual and vestibular motion cues were given to the subject, and his compensatory behavior used to infer his perception of self-motion. Such an approach avoids magnitude estimation as such, since the subject's objective is one of simply matching sensation with the sensation of sitting still.

This approach has its own drawback, however, since the tracking dynamics of the human operator are imbedded in the results. To provide an operator correction, an initial experiment determined the operator describing function, under conditions functionally similar to those used in the motion sensation experiments. This is described immediately below, following which will be discussed the results of two experiments aimed directly at developing a dual-input functional model of motion sensation.

4.0 Human Operator Dynamics

4.1 Experimental Design

Operator behavior was measured in nulling the velocity of a projected stripe pattern on the translucent front window of a small aircraft trainer. The pattern consisted of alternating black and white vertical stripes, subtending 12° each and filling approximately 60° of the subject's frontal visual field. This arrangement minimized the possibility of circularvection (6); further, the trainer remained stationary throughout the task, and the subject was informed of this prior to the experiment. No sensation of self-motion arose, as indicated by post-test questioning of the subjects.

Figure 1 is a block diagram of the nulling task, with the subject represented (within the dashed line) as a linear operator with remnant. It is presumed that the subject generates an internal estimate of visual field velocity, through an accurate estimator which is fast with respect to the motion sensation dynamics we are trying to investigate; hence the unity gain. A negative feedback structure for the subject is also presumed, with the velocity estimate subtracted from the task objective to generate an error signal for control action.
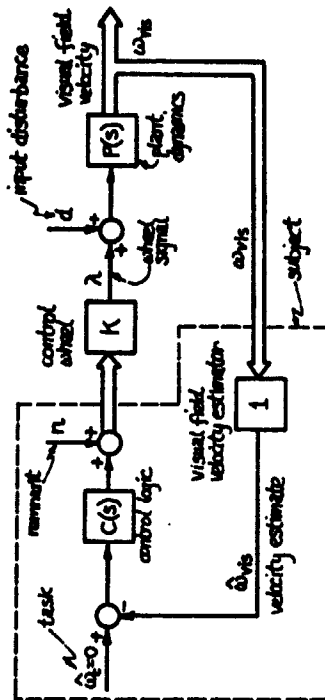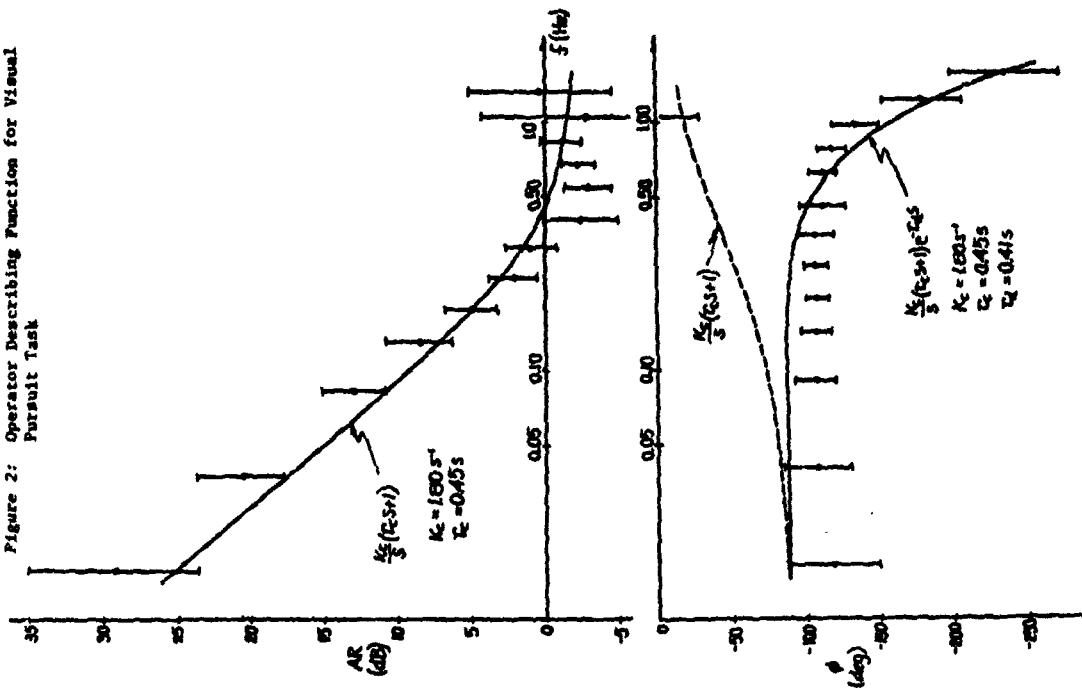

Figure 1: Visual Field Velocity Nulling Task

Figure 2: Operator Describing Function for Visual Pursuit Task

The subject controls field velocity via a wheel mounted horizontally in front of him; the wheel has no mechanical centering cues and is effectively featureless, providing neither visual nor tactile cues as to true center. Full deflection results in maximum field speed of $20°/s$, in the direction of wheel rotation. As shown in the figure, the wheel signal is added to a loop disturbance signal, against which the subject must provide compensatory control. The disturbance is a pseudo-random zero mean signal with a period of 128 seconds, consisting of a sum of 13 sinusoids spanning the frequency range from 0.01 to 1.0 Hz. The disturbance line spectrum follows that of a double lag-lead with a roll-off at 0.15 Hz, dropping 20 dB to level off a, 0.48 Hz. The combined wheel and disturbance signal are then passed through simulated plant dynamics, given by:

$$P(s) = \omega_n^2/[(s^2 + 2\zeta_n\omega_n s + \omega_n^2] \qquad (\omega_n, \zeta_n) = (5.65, 0.7) \qquad [1]$$

The output of this filter is then used to command a servo-driven projection system responsible for generating the front window moving stripe pattern.

4.2 Results

Six subjects attempted to maintain zero field velocity for two full presentations of the disturbance signal. Fast Fourier Transforms (FFTs) were performed on the wheel deflection and field velocity histories, and gain and phase were computed according to:

$$|\hat{A}(s)/\omega(s)|_{s=i2\pi f_i} \qquad [2]$$

where the f_i are the frequencies contained in the disturbance d. Figure 2 shows the six subject average Bode plots, with one-sigma deviations indicated by error bars. Also shown is a least-squares fit, to the gain data, of the following function

$$C(s) = \frac{K_c}{s}(\tau_c s + 1)e^{-\tau_d s} \qquad K_c = 1.80\ s^{-1},\ \tau_c = 0.45\ s, \qquad [3]$$
$$\tau_d = 0.41\ s$$

The dead-time τ_d was calculated from a least squares fit to the phase residuals based on the gain fit. Remnant corrections to the data were calculated according to the method suggested by Shirley (13), but were not found to significantly change the parameter values of the subsequently fitted transfer function. Although the fit could certainly be improved by the choice of a higher order transfer function, the simplified operator model of [3] is adequate for the purpose of the analysis to follow.

5.0 Visual Cues and Low Frequency Sensation

Our initial objective was to verify the hypothesis of frequency separation during sensory processing of simultaneous visual and vestibular motion cues. Specifically, we wished to demonstrate how low-frequency visual cues dominate low-frequency sensations, and how they can be used to augment the AC vestibular transduction characteristics of the vestibular system.

Figure 3: Closed-loop Velocity Nulling Task (Single Disturbance Input).

5.1 Experimental Design

Motion sensation was measured by giving the subject the task of nulling his own sense of self-motion, and effected by providing him with active control over his actual velocity, while seated in a LINK GAT-1 small aircraft trainer, modified for use as a simple velocity servo in yaw. Figure 3 is a block diagram of the experiment with the same type of schematic representation of the subject used earlier. The model proposes that the subject processes both visual and vestibular cues to arrive at an estimate of self-velocity, which, in turn, is used as a basis for providing compensatory wheel deflections. The wheel signal is combined with the same type of disturbance signal used in the previous experiment (pseudo-random, zero mean), although for this experiment a shelf spectrum is used to define the sinusoid amplitudes, with a corner frequency of 0.25 Hz and a 20 dB gain drop from high to low frequencies. This pseudo-random disturbance requires the subject to provide continuous compensation throughout a run. The combined wheel and disturbance signal then commands the trainer, used simply as a velocity servo in yaw and having the same second-order dynamics which were simulated in the previous experiment (P(s) defined by [1]).

The front window of the trainer is made opaque and the two translucent side windows are used for presenting the vertical stripe pattern to the subject's peripheral field. Field velocity can be directly controlled, since the projection system is mounted on the trainer. The optics are arranged so that as the pattern moves forward on one side window, it moves aft on the other, mimicking the rotational movement one would see inside a cylindrical drum.

The figure indicates a switch for presenting the subject with three types of visual field motion. In the CTR position, a tachometer feedback from the trainer counterrotates the visual field with respect to the trainer, providing moving-base isolation for the field. The subject sees the field as effectively fixed in space, and thus this mode mimics the everyday correspondence between visual and vestibular cues. In the FIX position, the field is fixed with respect to the trainer, depriving the subject of any visual motion cues. Finally, in the CV position, the field is driven at constant velocity with respect to the trainer, 4°/s to the right; this would normally induce a left CV sensation in a motionless subject.

5.2 Experimental Protocol

Six subjects participated in the experiment. All were in normal health with normal peripheral vision, and had no known vestibular dysfunction. Each subject was specifically told to keep the trainer as motionless as possible, by concentrating on his own sensation of motion and providing the appropriate compensatory wheel deflections. Each subject was then given a practice session of two minutes, under counterrotating field conditions. Headphones were used to mask auditory cues, and a head rest provided head stabilization with respect to the trainer. Subjects were instructed to look forward, but not to the extent of fixing their gaze on a specific point.
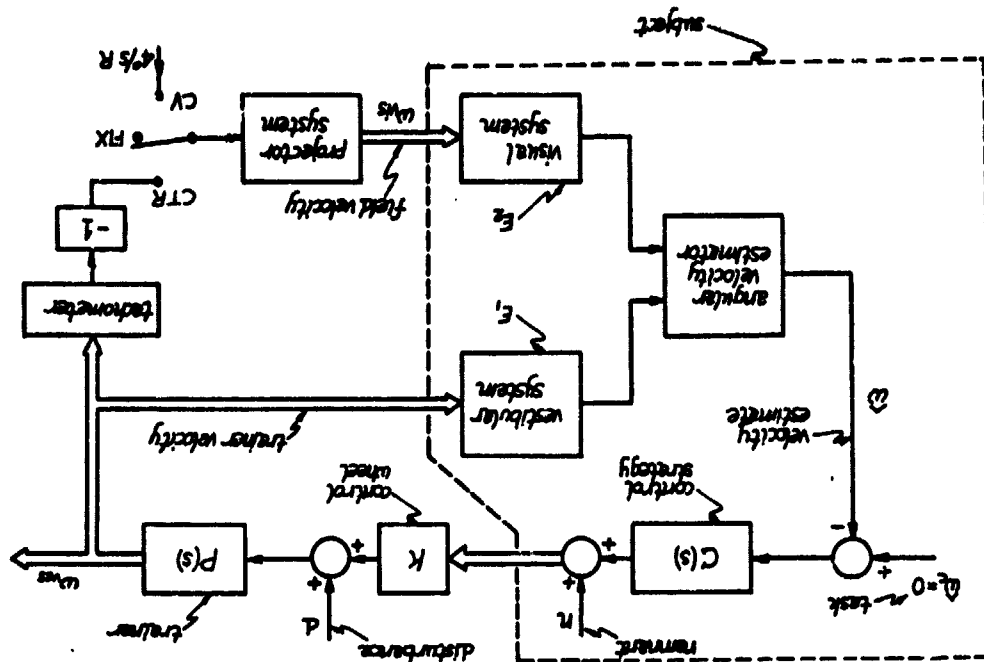
A typical run lasted for approximately 12 minutes, during which time the subject was required to provide continuous velocity-nulling compensation. During this period, each of the three visual field conditions (CTR, FIX and CV) was repeatedly presented to the subject in random order, the start of each presentation synchronized with the disturbance signal (T = 128 s). Each field presentation lasted for 128 seconds, unless stick saturation necessitated early termination of the stimulus.

5.3 Results

Figure 4 shows one subject's strip chart recording of the disturbance signal and three trainer velocity histories, one for each visual field conditions type. Under counterrotating field conditions (CTR), the mean trainer velocity was maintained near zero by all subjects, with an RMS error, for the population of 1.34°/s. Under fixed field conditions (FIX), subjects drifted away from zero, either left or right, at a constant steady acceleration ($\bar{a} = 0.011°/s^2$, $\sigma_a = 0.050°/s^2$) (typical vestibular thresholds in yaw rotation are 0.1 to 0.29°/s²). Over the population, the mean acceleration are significantly different from zero, indicating a left-right balance in the population. With a constant velocity field presentation (CV), all subjects accelerated to the right, at a rate ($\bar{a} = 0.29°/s$, $\sigma_a = 0.21°/s^2$) significantly larger than that seen in the FIX presentations ($p < 0.005$). It should be noted that in all of the field presentations, the subjects felt that they were maintaining themselves at zero mean velocity, in spite of the supra-threshold accelerations they sometimes subjected themselves to.

5.4 Low Frequency Response

Some additional points regarding the field effects on motion are worth noting. With a counterrotating field, the subject successfully performs the task, as expected. This is the "normal" cue situation, in which visual and vestibular cues complement one another, and presumably provide an accurate velocity estimate. With a fixed field, one might be tempted to explain the observed drift as simply subthreshold acceleration; however, the fact that a subject's mean acceleration remains constant argues against this, since, presumably, any subthreshold acceleration profile would be just as likely. A more promising candidate to explain the observed drift is a vestibular "bias". Finally, with a constant velocity field, all subjects chase the field to the right, suggesting that the circularvection illusion is influencing the subject into thinking he is moving to the left, and leading him to provide inappropriate rightward compensation. Presumably, the left CV illusion and right vestibular acceleration cancel each other out, on the average.

Figure 4: Trainer Velocity Drift as a Function of Visual Field Type

VES

CTR

FIX

CV
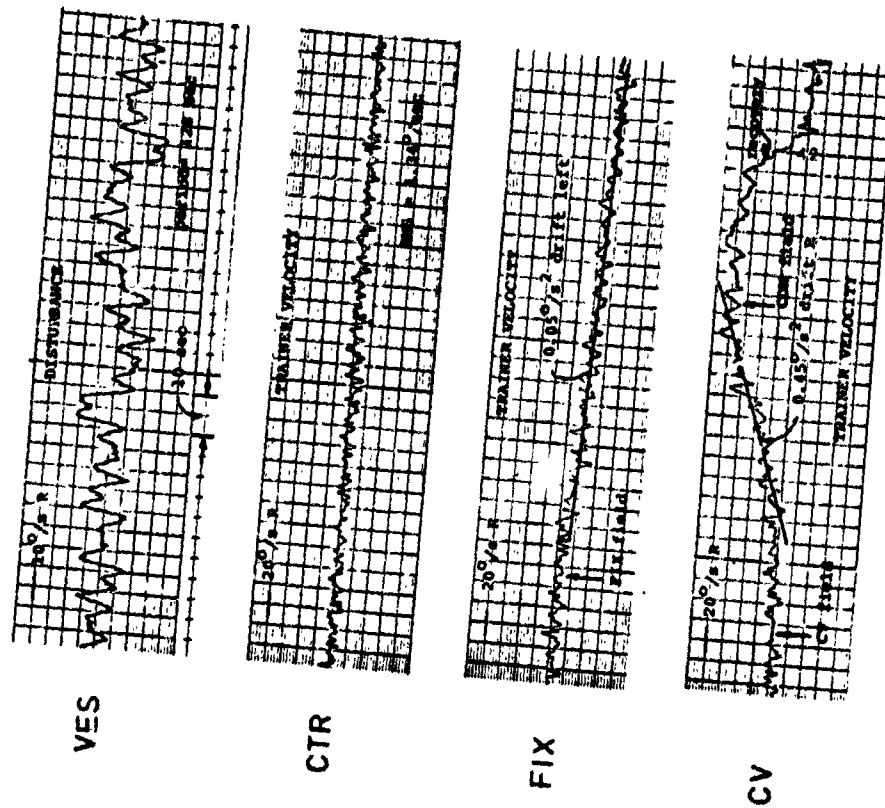
5.3 Low Frequency Response Model

A simple estimator model consistent with the experimental findings is illustrated in Figure 5. The vestibular path is based on the familiar cyclopean torsion pendulum model (14) with slow and fast time constants τ_1 and τ_2 respectively. The long vestibular adaptation time constant is ignored. Provision is made for a biased output ω_b, which is assumed constant in the analysis following. The visual path is modelled as a linear filter of unspecified dynamics, having a unity DC gain.
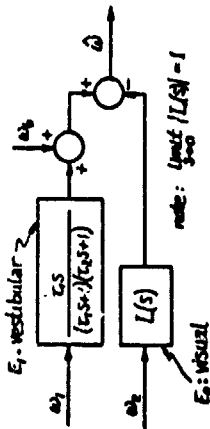

note: $\lim_{s\to 0} |L(s)| = 1$

Figure 5: Dual-Input Velocity Estimator (LF)

Under fixed field conditions (FIX), the model predicts a constant average trainer acceleration in the nulling task. To illustrate this, the estimator above may be combined with the loop diagram of Figure 3. Block diagram manipulation then yields the following expression for trainer velocity as a function of bias, disturbance, and remnant:

$$\omega_1(s) = \frac{P}{1 + PCE_1}(-C\omega_b + d + n) \quad [4]$$

assuming unity control wheel gain. Since we are interested in low-frequency behavior, we recall, from (1), that the plant P has unity DC gain; that, from [3], the control strat C behaves as an integrator (K_c/s); and that, from Figure 5, the vestibular estimator E_1 behaves as a differentiator ($\tau_1 s$). In terms of DC signal content, the bias ω_b is modelled as a constant (ω_b/s). Further, since the disturbance d is zero mean and the remnant n is assumed to contain no DC power, neither of these loop inputs contributes to low frequency response. The model thus predicts, from [4], a ramp in trainer velocity:

$$\lim_{s\to 0} \omega_1(s) = \lim_{s\to 0} -\kappa(\omega_b/s^2) \quad [5]$$

where we have defined the loop gain κ to be

$$\kappa \equiv K_c/(1 + K_c\tau_1) \quad [6]$$

In other words, the model predicts a steady trainer acceleration under FIX conditions, a_{FIX}, given by

$$a_{FIX} = -\kappa\omega_b \quad [7a]$$

A similar derivation may be used to show that, under constant velocity field conditions (CV), the model again predicts a steady trainer acceleration:

$$a_{CV} = a_{FIX} + \kappa\omega_{VIS} \quad [7b]$$

Finally, under counterrotating field conditions (CTR), the model predicts no steady trainer acceleration; instead, a trainer velocity bias, equal and opposite to the subject's vestibular bias, is predicted:

$$\omega_{CTR} = -\omega_b \quad [7c]$$

Although these results qualitatively agree with the observed behavior, it is of interest to consider some quantitative aspects of the model's predictions.

Clearly the gain factor κ varies among individuals, but a rough estimate can be obtained from [7b] by using the mean drift rates observed under FIX and CV conditions (in section 5.3), and using the fact that the CV field speed was 4°/s:

$$\kappa = 0.073 \text{ s}^{-1} \quad [8]$$

Assuming κ is constant across the population and using the observed FIX drift rate statistics (section 5.3), we can then use [7a] to calculate the model's vestibular bias statistics:

$$\bar{\omega}_b = 0$$
$$\sigma_{\omega_b} = 0.68°/s \quad [9]$$

It should be recognized that a subject with a three-sigma bias still perceives himself stationary in space, during the nulling task, since his steady state self-velocity estimate is given by

$$\hat{\omega}_{ss} = (\kappa/K_c)\omega_b - (\kappa/K_c)(3\sigma_{\omega_b}) = 0.06°/s \quad [10]$$

where we have used the value of K_c given in (1).

In summary, when the subject is deprived of visual motion cues, and feels himself stationary, the model ascribes the observed constant trainer acceleration to a bilateral vestibular bias, a bias not inconsistent with the motion of a left-right canal imbalance (14). Under counterrotating field conditions, this bias model also predicts, from [7c] and [9], one-sigma trainer velocity offsets of less than 1°/s, entirely consistent with the observed behavior.

Figure 6: Closed Loop Velocity Nulling Task (Dual Disturbance Input)

note : $P(s) = F(s)G(s)$

$\Phi_{d_1 d_2} = 0$
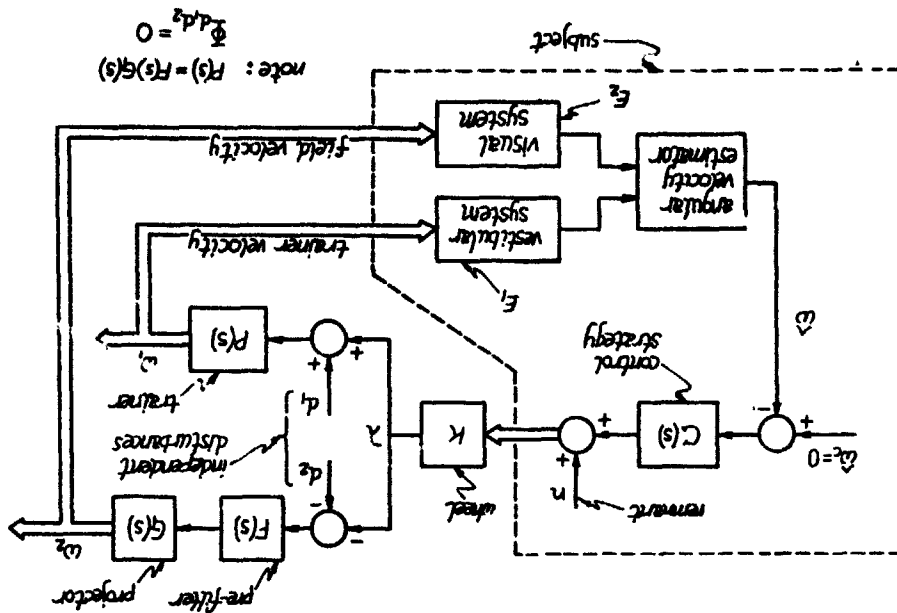
The model also allows us to estimate the "slow" vestibular time constant τ_1. From the definition of κ given in [6], its computed value in [8], and the value of K_c in [3], we find

$$\tau_1 = 13.1 \text{ s} \qquad [11]$$

The agreement between this computed value and the 10 to 15 second range found by other researchers (15) lends additional support to this dual-channel model.

6.0 Combined Cues and Dynamic Motion Sensation

To look more closely at what is essentially a dynamic dual-input problem, a third experiment was performed to see if the above parallel-channel model could be extended to account for the subject's dynamic behavior. The approach chosen was to work with two describing functions: one relating trainer motion to wheel deflection and the other relating visual field motion to wheel deflection.

6.1 Experimental Design

The same velocity nulling task as in the second experiment was given the subject: that is, to keep himself fixed in space. Instead of having him control only trainer velocity, however, he was also given control of field velocity. This allowed him to null either vestibularly-induced or visually-induced motion sensations by using the control wheel appropriately. Disturbance signals were injected into both the trainer and projector drives, requiring constant compensation. By choosing the disturbance signals to be uncorrelated, simultaneous nulling of both cues becomes an impossible task objective. Clearly, the resulting analysis will be based on whichever portion of which the subject chooses to null.

Figure 6 is a functional block diagram of the experiment, with the same type of schematic model of the human operator introduced earlier. Trainer velocity is as in the previous experiment. Field velocity, however, is determined by both wheel deflection and the second disturbance input. It should be noted that the sign of the wheel signal is changed prior to being sent to the projector drive, to make the resulting visual field motion consistent with trainer motion (i.e. right wheel deflection results in right trainer motion and left field motion). To ensure that the visual field dynamics mimic trainer response, a prefilter was added to the projector drive (which has a relatively high bandwidth), so that, as shown on the figure, FG = P. Thus, without a visual field disturbance signal, the experiment would be functionally equivalent to the counterrotating series conducted earlier.

6.2 Identification Method

It is appropriate to consider how an estimator model can be derived from

the results of this experiment. We assume that the velocity estimate is a linear function of the two cues, but presume no particular channel dynamics:

$$\hat{\omega} = E_1(s)\omega_1 + E_2(s)\omega_2 \quad [12]$$

where ω_1 is the trainer velocity, and ω_2 is the visual field velocity with respect to the trainer (and object). If we define the remnant (n) to be uncorrelated with the input disturbances,

$$\Phi_{nd_1} = \Phi_{nd_2} = 0 \quad [13]$$

and choose the disturbances to be uncorrelated:

$$\Phi_{d_1d_2} = \Phi_{d_2d_1} = 0 \quad [14]$$

then, block diagram calculation using Figure 6 shows that:

$$\Phi_{\hat{\omega}d_1}/\Phi_{\omega_1d_1} = -CE_1/(1 + PCE_2) \quad [15a]$$

$$\Phi_{\hat{\omega}d_2}/\Phi_{\omega_2d_2} = CE_2/(1 + PCE_1) \quad [15b]$$

Since the left-hand side is computable from experimentally measured variables, we define

$$\alpha_1 \equiv \Phi_{\hat{\omega}d_1}/\Phi_{\omega_1d_1} \qquad \alpha_2 \equiv \Phi_{\hat{\omega}d_2}/\Phi_{\omega_2d_2} \quad [16]$$

so that one can compute the operator transfer functions:

$$CE_1 = \alpha_1(1 + P\alpha_2)/(1 + P^2\alpha_1\alpha_2) \quad [17a]$$

$$CE_2 = \alpha_2(1 - P\alpha_1)/(1 + P^2\alpha_1\alpha_2) \quad [17b]$$

As expected, the control strategy C is inseparable from the estimator transfer functions, E_1 and E_2.

Rather than work with cross-power spectral densities, it was found computationally more convenient to use conventional input-output calculations based on Fourier transforms of the signals themselves. Thus, if f_{ij} is a frequency contained in the loop disturbance d_i, then the α_i are calculated according to

$$\alpha_i(f_{ij}) = \hat{\omega}(f_{ij})/\omega_i(f_{ij}) \qquad (i = 1,2)\ (\forall_j) \quad [18]$$

The direct correspondence with [16] is made possible by the

independence of d_1 and d_2, and the assumption of a small remnant contribution at the disturbance frequencies. Since [17] requires that α_1 and α_2 be defined at the same set of frequencies, linear interpolation in the frequency domain is used to generate additional values of the α_i; these are then used in [17] to calculate the CE_i.

6.3 Experimental Protocol

Six subjects participated in the experiment. After a familiarization period with the procedure and equipment, each subject performed one continuous run of velocity nulling which lasted for approximately eight minutes. The visual environment alternated between two modes: the counterrotating field mode (CTR) which provides accurate confirmation of vestibular cues, and the dual-input mode (DI) illustrated in Figure 6. Two presentations of each were given, alternating with one another:

            Series A: CTR, DI, CTR, DI
            Series B: DI, CTR, DI, CTR

Three subjects received series A and three received series B, to provide balance for fatigue and learning.

6.4 Results

After performing FFTs on the histories of the wheel deflection, trainer velocity and field velocity, the operator transfer functions were computed according to [17], at each disturbance frequency. The resulting six-subject gain and phase averages are given in Figure 7, along with smooth curves sketched in to indicate trends with frequency. Several points are worth noting. First, the "vestibular" gain follows what might be expected from a lag-lead, augmented by a lead at high frequencies and a washout at low frequencies. This washout characteristic is entirely consistent with our notion of negligible canal response at low frequencies, and, of course, is consistent with the functional model presented earlier.

The Bode plots defining the visual transfer function, CE_2, show quite contrasting behavior. At low frequencies, the gain is higher than in the vestibular channel, supporting the drift rate findings in which the dominance of a DC visual cue was demonstrated. Up to approximately 0.1 Hz, the visual channel behaves as a simple integrator (in gain and phase), which, as might be surmised from the manual control results, is simply a reflection of the operator's control dynamics. Although the visual gain levels off at about 0.1 Hz, it remains considerably smaller (≈ 10 dB) than the vestibular gain, at frequencies above the gain crossover point (f ≈ 0.02 Hz). The complementary filter hypothesis thus appears quite attractive.

Four of the subjects participated in both the manual control task and in the current experiment. Thus, for each individual, at each test frequency, the gain and phase data (CE_i) can be adjusted by the gain and phase data
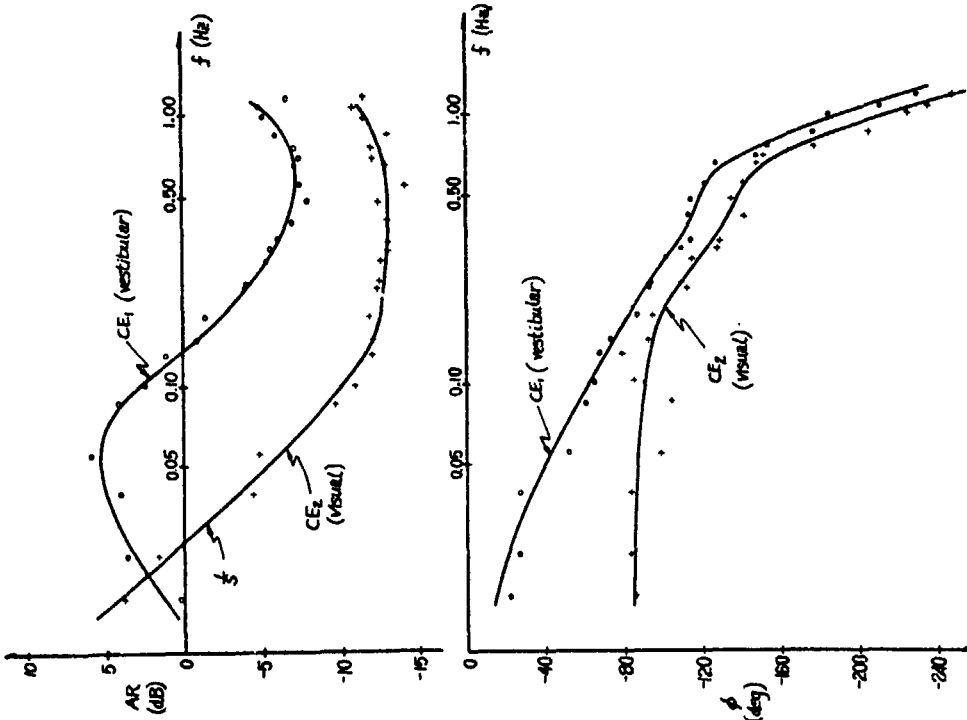
defining that subject's operator dynamics (C), obtained from the manual control experiment. Shown in figures 8a and 8b are the resulting estimator describing function data for E₁ and E₂, obtained by averaging over the four subject population. Also shown are smooth curves associated with two linear transfer functions which provide a least squares fit to the data.

The vestibular channel data (figure 8a) exhibit, at first glance, the AC characteristics we would associate with the canals: both the rapid gain drop and phase lead with decreasing frequency are qualitatively well-modelled by a washout filter. However, the break frequency is quite high: the washout time constant is 0.94 s from the fit, which is an order of magnitude smaller than the 10 s time constant we would expect from the canals (16). The discrepancy is even larger when compared with the 13.1 s value calculated from drift measurements. Finally, it is appropriate to note that we might expect unity gain at the high test frequencies; the data in contrast, is better fit with half that gain.

The visual gain (figure 8b) is a good deal lower than the vestibular gain, over much of the frequency range, with crossover occurring at the very low end (f ≈ 0.02 Hz). In this region, the gain is approximately constant with frequency, behavior which is qualitatively consistent with the idea of DC visual cue dominance. However, we might expect the DC gain to be approximately unity; certainly not the -25 dB seen in the data. Furthermore, if the visual channel were to be truly complementary to the vestibular channel, we would expect a roll-off near 0.1 Hz. Just the opposite occurs, however.

These results suggest a reevaluation of a linear dual channel model for cue mixing.

7.0 Non-Linear Dual Channel Model

The obvious means of resolving the apparent inconsistencies just d . . . . r is to propose that simultaneous cue presentation involves a mixing ... two cues at different frequencies: that is, allowing a vestibular cue at one frequency to affect a visual cue at another, and vice versa. A non-linear model is clearly called for, and a reasonable foundation on which to build has already been provided by the "conflict model" hypothesis (10), which proposes that each cue be weighted according to the perceived conflict between them. (The notion of a switching mechanism between visual and vestibular influences on vestibular unit activity was also discussed by Waespe and Henn (4)).

One implementation of this hypothesis is shown in figure 9a, in which the visual and vestibular cues are weighted in a complementary fashion according to the gain K. This gain is dependent on a measure of cue conflict, ω_{err}, which, in turn, is derived directly from the two cues. The vestibular sensory dynamics are approximated by the low frequency portion of the torsion pendulum model. No visual sensory dynamics are modelled, for two reasons: the lack of experimental data for single channel visual cue response, and the known relatively wide-band motion detection response of the visual system.

Figure 7: Dual-Input Describing Functions (uncorrected for operator dynamics)
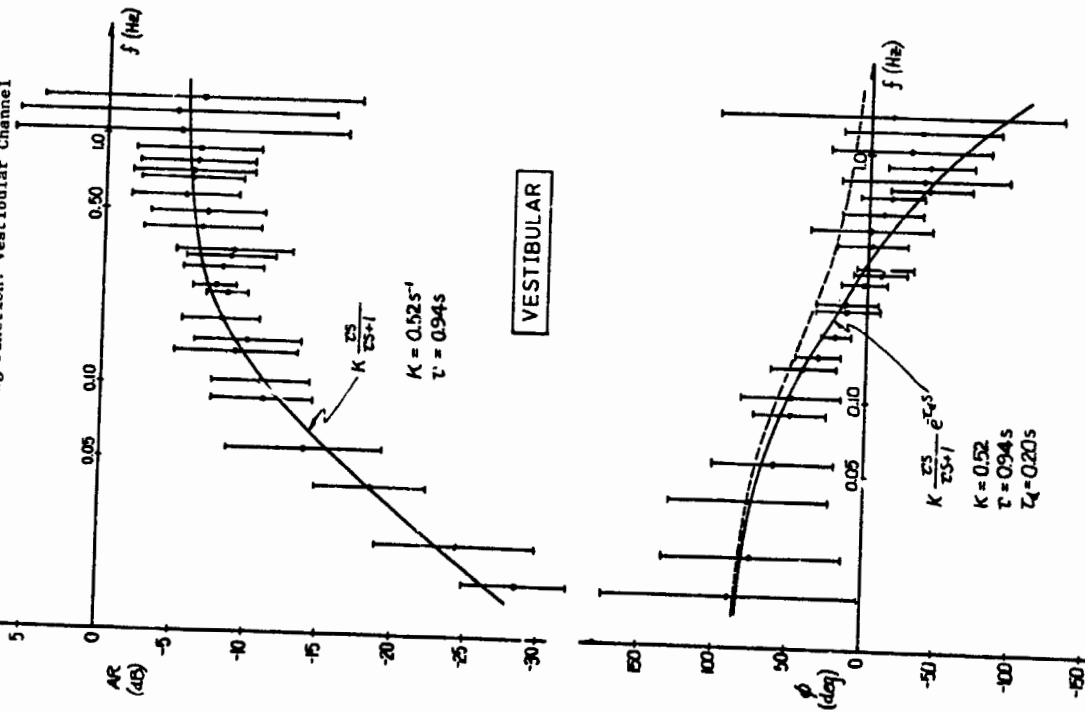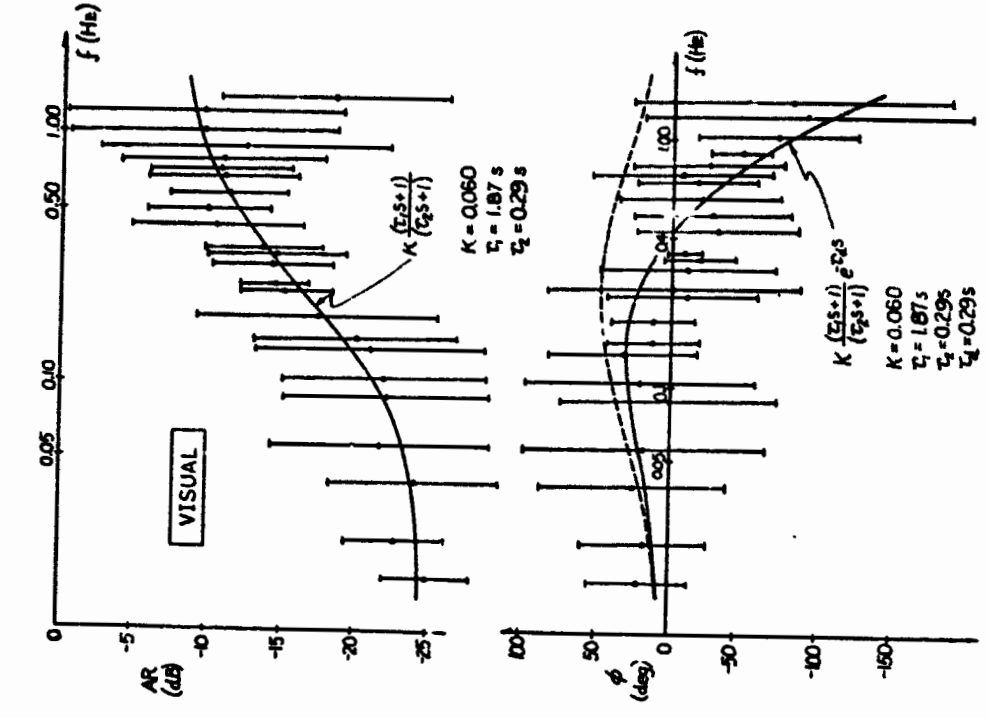
Figure 8b: Dual-Input Describing Function: Visual Channel

VISUAL

$$K\frac{(\tau_1 s+1)}{(\tau_2 s+1)}$$

$K = 0.060$
$\tau_1 = 1.87\,s$
$\tau_2 = 0.29\,s$

AR (dB)

f (Hz)

$$K\frac{(\tau_1 s+1)}{(\tau_2 s+1)}e^{-\tau_3 s}$$

$K = 0.060$
$\tau_1 = 1.87\,s$
$\tau_2 = 0.29\,s$
$\tau_3 = 0.29\,s$

ϕ (deg)

f (Hz)

Figure 8a: Dual-Input Describing Function: Vestibular Channel

VESTIBULAR

$$K\frac{\tau_1 s}{\tau_2 s+1}$$

$K = 0.52\,s^{-1}$
$\tau' = 0.94\,s$

AR (dB)

f (Hz)

$$K\frac{\tau_1 s}{\tau_2 s+1}e^{-\tau_4 s}$$

$K = 0.52$
$\tau' = 0.94\,s$
$\tau_4 = 0.20\,s$

ϕ (deg)

f (Hz)

A simple conflict measure can be motivated by considering, for example, self-motion in an inertially-fixed visual field environment. Although this is clearly a zero conflict situation, a direct comparison of the two cues would lead to a discrepancy, because of the differences in the dynamic response of the two sensory channels. One is thus led to propose an internal model of canal dynamics, through which the visual information can be passed to provide a predicted vestibular response, which can then be compared with the actual vestibular signal. Effectively, then, conflict would be based on high frequency cue content.

A weighting schema can then be proposed fairly directly. Since the conflict signal is a measure of high frequency agreement, and the vestibular system provides "reliable" information at high frequency, then it would seem reasonable to heavily weight this information whenever a high conflict situation is detected. The converse might be proposed with low conflict: heavily weight the visual cue. However, this approach is only reasonable at low frequencies, when we know the vestibular channel will be providing a null signal. At high frequencies, this weighting discards confirming vestibular information which clearly could be used to improve the velocity estimate. With no apriori knowledge of each channel's noise characteristics, an estimate can be obtained by simply averaging the cues. Thus, in a low conflict situation, we propose cue averaging, unless we have a zero vestibular signal, in which case we heavily weight the visual cue.

An implementation of this type of conflict measure and weighting schema is shown in Figure 9b. The visual cue is high-passed through an internal model of the vestibular dynamics to generate an expected vestibular signal ω_{exp} which is then differenced with the actual vestibular signal and passed through a rectifier. To allow for a long term resolution of steady state conflict, an adaptation operator acts on the rectified signal to generate the actual conflict signal, ω_{err}.

The symmetric weighting function is implemented with a cosine bell. As illustrated, a large conflict signal drives the visual path gain to zero, whereas a small one drives it to a peak weighting value which varies between 1/2 and 1, depending on the amplitude of the vestibular signal (and implemented via an additional bell function). Thus, in a low conflict situation, the cues can either be averaged or the visual cue passed straight through, depending on whether or not the vestibular signal is large or small, respectively.

7.1 Dynamic Behavior of the Nonlinear Model

The non-linear model was simulated on a digital computer, to evaluate predicted response as a function of cue presentation. The results presented here are preliminary, in that no exhaustive parameter searches have been conducted to provide a best fit to the data; however, the trends predicted by the model deserve some comment as they may motivate a closer look at the details of future model implementation.
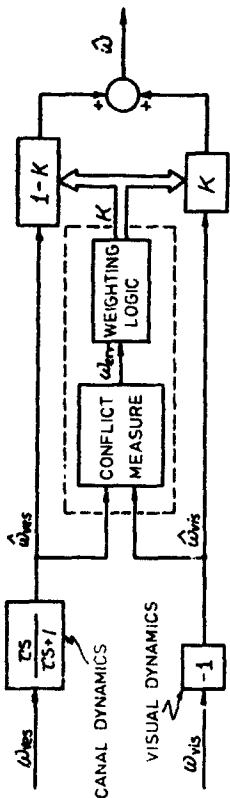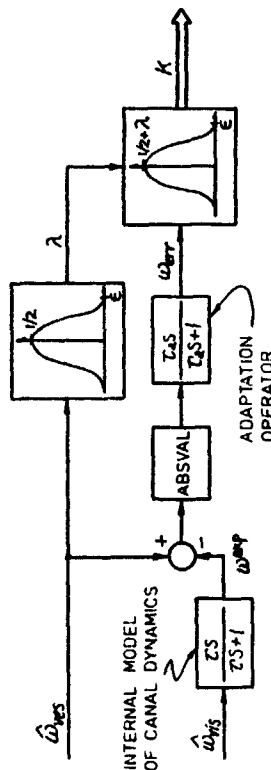
Figure 9a: Dual input conflict model

Figure 9b: Conflict measure and weighting function

Figure 10d: Response to Visual Step and Vestibular Ramp

Figure 10b: Visual Step Response

Figure 10c: Response to Visual and Vestibular Steps.

Figure 10a: Vestibular Step Response

Three parameters determine model behavior. For the simulations, the vestibular time constant, τ, was assigned the 13.1 s value found from the CV drift rate of section 5.5. The adaptation time constant Ta was chosen to be 10 s, which is the order of magnitude of the acceleration latencies observed when subjects were presented with a constant velocity field rotation. The presumption here is that the latency is due, in part, to the unresolved conflict between the subject's CV illusion (left) and his sensed acceleration (right), a conflict which must eventually be washed out by the adaptation operator. Finally, the velocity magnitude measure, ε, was chosen to equal the Meulder product (16) of $2.5°/s$, the presumption being conflict detection may be characterized by the same type of threshold behavior associated with vestibular pulse detection.

7.2 Time Response

Shown in Figures 10a through d are time histories of the model's response to simple visual and vestibular cues. Figure 10a is the model's prediction of subjective response to a $5°/s$ step in angular velocity, with a subject-fixed visual field. Although the response appears to be characterized by two exponentials, only the first portion is truly exponential, and is due to the fact that the canals provide the only information during the initial high conflict phase. As the conflict decreases with time, the null visual signal is weighted more heavily, and the response thus decays more rapidly. A similar double branch decay, following a velocity step, is seen in the velocity of slow phase nystagmus (V. Henn, personal communication). Figure 10b shows model response to a left $4°/s$ step in visual field velocity, in the absence of confirming vestibular cues. Again, because of the initially high conflict level, the null vestibular cue is the basis for sensation resulting in the response latency seen. As the expected vestibular signal drops to zero and matches the actual null signal from the canals, the conflict lessens and the weighting on the visual cue increases to unity (the undershoot is caused by the adaptation operator acting on the conflict signal, temporarily increasing the conflict level).

Figure 10c shows the model response to confirming visual and vestibular velocity steps (CVP presentation). Since this is a zero conflict situation, the initially large vestibular signal dictates that both cues be averaged, which results in a sensation drop-off due to the decaying canal response. As the vestibular signal grows smaller, however, the weighting emphasizes the DC visual cue, bringing the subjective response back to the true velocity level. Figure 10d shows model response to a constant field velocity of $4°/s$ combined with a constant body acceleration of $0.3°/s^2$, both to the right. The initial response is due to the vestibular path, but is turned around as the oppositely-directed circularvection illusion takes hold. The conflict gradually decreases, because of the adaptation operator, but the vestibular signal remains at a constant level ($\tau a = 4°/s$), so that, in the steady state, both cues are averaged. The net result is approximately zero sensation, and agrees with what is observed experimentally, under CV visual field conditions (recall section 5.3).
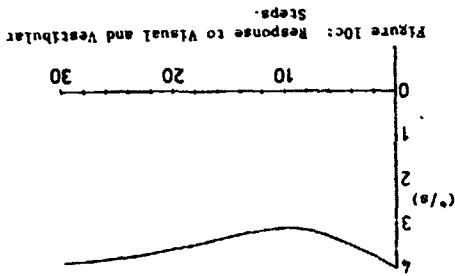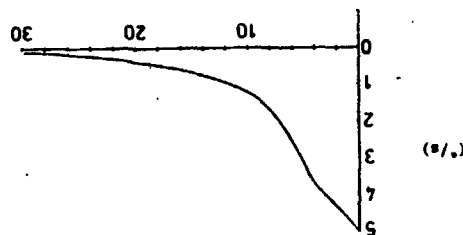
Figure 11: DI experimental data compared with simulated conflict model response
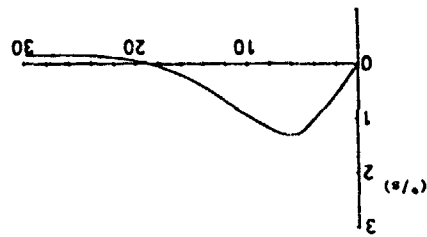
VESTIBULAR
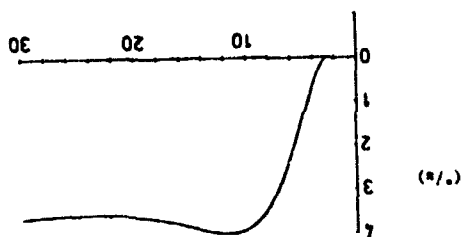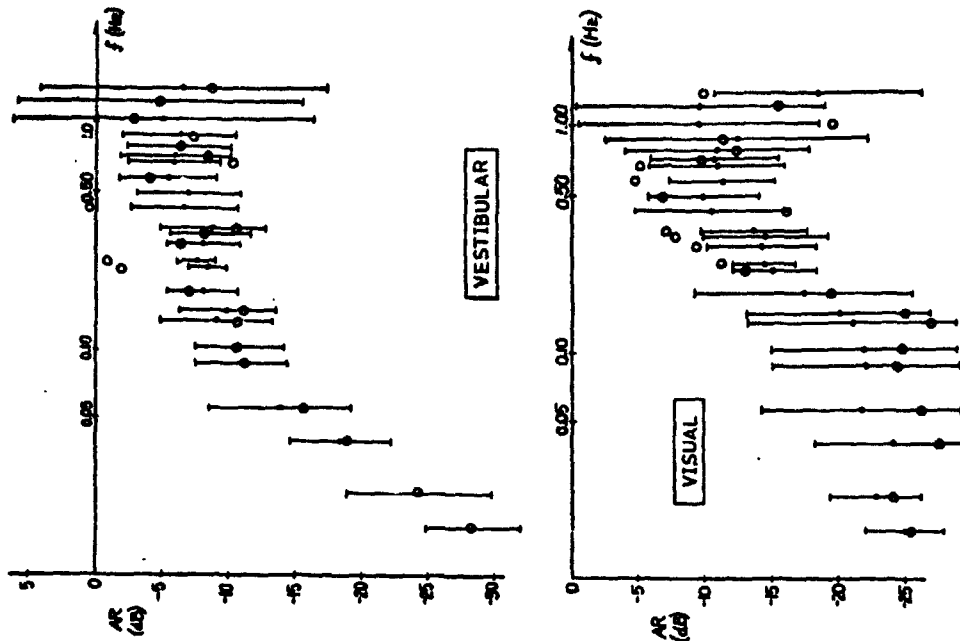
VISUAL

7.3 Frequency Response

Although the model appears to provide reasonable predictions of subjective response to simple cue presentations, of perhaps greater interest is its ability to fit the apparently inconsistent data obtained from the dual input pulling task. A digital simulation of the DI experiment was conducted using the same plant dynamics and loop disturbances as in the experiment. The subject was simulated as shown schematically in Figure 6, using the control strategy of [3] and the non-linear estimator of Figure 9. The simulation ran for one period of the disturbance signal and the simulated trainer, visual field, and wheel histories were processed with the same software used for the experimental data analysis.

Repeated in figure 11 are the visual and vestibular gain plots obtained from the experiment; the superimposed open circles are the gains for the simulated non-linear estimators. A comparison with the earlier linear system fit makes it clear that the non-linear model does a poorer job of fitting the experimental data; however, since the linear model is untenable due to our previous considerations, this only suggests that there is room for improvement in the non-linear estimator. As it stands, however, the major data trends are reasonably well-followed by the model. In particular, the 13.1 s vestibular time constant is transformed to an effective one-second time constant by the conflicting visual cues. Similarly, conflicting vestibular cues effectively drop the unity gain of the visual channel by 25 dB, at low frequencies; at higher frequencies, the conflict lessens because of the decreased magnitudes of the loop disturbances, and the visual gain rises. The gain rise thus no longer needs to be attributed to high frequency visual lead, a dynamic characteristic inconsistent with our knowledge of circularvection response. Thus, the non-linear model provides a means of fitting the dual input results, while allowing for consistency with single stimulus experiments.

8.0 Summary

This study has confirmed the notion that we estimate self-motion by combining complementary visual and motion cues: low frequency visual cues are used to augment high frequency vestibular cues to effect a wide-band sensory system. Although a linear complementary filter provides an adequate functional description of low frequency behavior, the dual-input experiment reported on here shows that the assumption of linearity leads to model predictions which are inconsistent with the results of single cue experiments. The non-linear model proposed here circumvents these apparent inconsistencies by recognizing that cue conflict provides a means by which the two cues can be selectively weighted to arrive at a "best" estimate of self-motion.

401

REFERENCES

1. Henn, V., Young, L.R., Finley, C. "Vestibular nuclear units in alert monkeys are also influenced by moving visual fields", Brain Research 71:144-9, 1974.

2. Dichgans, J., Schmidt, C.L., Graf, W. "Visual input improves the speedometer function of the vestibular nuclei in the goldfish", Exp Brain Research 18:319-322, 1973.

3. Allum, J.H.J., Graf, W., Dichgans, J., Schmidt, C.L. "Visual-vestibular interactions in the vestibular nuclei of the goldfish", Exp Brain Research 26:463-485, 1976.

4. Waespe, W., Henn, V. "Neuronal activity in the vestibular nuclei of the alert monkey during vestibular and optokinetic stimulation", Exp Brain Research 27:523-538, 1977.

5. Daunton, N.G. and Thomsen, D.D. "Otolith-visual interactions in single units of cat vestibular nuclei. Neuroscience Abstracts, Volume II, part 2, p. 1057, 1976.

6. Brandt, Th., Dichgans, J., Koenig, E. "Differential effects of central versus peripheral vision on egocentric and exocentric motion perception", Exp Brain Research 16:476-491, 1973.

7. Young, L.R., Oman, C.M. "Influence of head position and field position on visually induced motion effects in three axes of rotation", Proceedings of the Tenth Annual Conference on Manual Control, 1974.

8. Young, L.R., Oman, C.M., Dichgans, J. "Influence of head orientation on visually induced pitch and roll sensation", Aviation Space Environ Med 46:264-268, 1975.

9. Young, L.R., Dichgans, J., Murphy, R. and Brandt, Th. "Interaction of opto-kinetic and vestibular stimuli in motion perception", Acta Otol 76:24-31, 1973.

10. Young, L.R., "On visual vestibular interaction", NASA Fifth Symposium on the Role of the Vestibular Organs in Space Exploration, NASA SP-314, 1970.

11. Berthoz, A., Pavard, B., Young, L.R. "Perception of linear horizontal self motion induced by peripheral vision (linearvection)" Exp Brain Research 23:471-489, 1975.

12. Poulton, E.C. "The new psychophysics: Six models for magnitude estimation" Psychol Bull 69:1-18, 1968.

13. Shirley, R. Motion Cues in Man Vehicle Control , Sc.D. Thesis, Department of Aeronautics and Astronautics, Massachusetts Institute of Technology, Cambridge, MA, 1968.

14. Young, L.R. "Dynamic control models of the semicircular canals", extension of "The current status of vestibular system models", Automatica, 5:369-383, 1969; Presented at the Seventh Annual Conference on Manual Control, 1971.

15. Melvill Jones, G., Barry, W., Kowalsky, N. "Dynamics of the semicircular canals compared in yaw, pitch and roll", Aerospace Med 35:984-989, 1964.

16. Oosterveld, W.J., "Threshold value for stimulation of the horizontal semicircular canals", Aerospace Med 41:386-389, 1970.